ELSEVIER

International Journal of Mass Spectrometry 181 (1998) 173–180

International Journal of Mass Spectrometry

Well defined chopping of the Paul trap rf potential up to a 1.5 MHz frequency combined with a time-of-flight method

J. Rocher, M. Vedel, F. Vedel*

Physique des Interactions Ioniques et Moléculaires (UMR 6633 CNRS-UAM1), Centre de St-Jérôme, Case C21, F13397, Marseille Cedex 20, France

Received 10 July 1998; accepted 13 September 1998

Abstract

A technique for extracting ions from a Paul trap is described wherein the trapping potential is interrupted sharply when crossing the zero value. A time-of-flight profile, corresponding to the ion cloud kinetic energy distribution at the instant of trapping potential interruption, has been observed from the subsequent free motion of the ions. Unavoidable residual overshoots of the storage voltage at this instant are taken into consideration in a three-dimensional (3D) simulation of 10^6 ion trajectories. Experimental profiles obtained with very good reproducibility can be matched with simulations (in the form of a histogram of ion number arriving at an electron-multiplier detector in successive intervals of time). The fitting is achieved by variation of the assumed ion kinetic energy and a coefficient representing the anisotropy of the ion cloud. It was found that experimental profiles obtained by this ejection method has been modeled to a radio frequency of 1.5 MHz corresponding to a confinement voltage of about 700 V_{pp}. The uncertainty on the fitting of the profiles presented here leads to uncertainties in energy evaluation situated between 0.1 and 0.3 eV. (Int J Mass Spectrom 181 (1998) 173–180) © 1998 Elsevier Science B.V.

Keywords: Paul trap; Kinetic energy measurements; TOF methods

1. Introduction

The Paul trap is an entirely appropriate device for the isolation of ionic species from external interactions. Furthermore, the characteristics and properties of such traps are well known. The Paul trap has been applied to numerous studies of gaseous ions ranging from physical chemistry [1] to the measurement of time and frequency [2]. A requirement common to all of these applications is a knowledge of the kinetic energy (or temperature) of the ion cloud. In experiments where laser spectroscopy is used, this requirement is satisfied directly by measuring the Doppler broadening of a spectral transition. In chemical applications, however, the Doppler method is usually not applicable for the determination of ion kinetic energies and, furthermore, the use of a chemical "thermometer" reaction, wherein the activation energies and thermochemistry are well known, is often not convenient. The most general method for ion kinetic energy determination consists of ejecting ions from the Paul trap by application of an extraction pulse to an end-cap electrode [3,4] and deducing subsequently the velocity distribution from the time-of-flight profile obtained from a detector. The difficulty of this method

* Corresponding author. E-mail: fern@frmrs12.u-3mrs.fr

PII S1387-3806(98)14185-4

is the simulation of the electric field generated by the application of the pulse since the symmetry of the potential applied to the trap is perturbed. Nevertheless, this method can be applied successfully to deduce from the time-of-flight the total ion number trapped on account of the large signal it allows to obtain.

A method that permits easier modeling is one where no additional voltage for ejection is used. This method consists of interrupting the storage field (oscillating at a frequency $\Omega/2\pi$) at a given instant in time (corresponding to a preselected rf phase) so that the voltage applied to the ion trap is frozen at any chosen value. In that way, the quadrupolar nature of the electric field is maintained and the influence on ion motion of the static field derived from this voltage is readily accounted for.

A method based on this principle [5] has been developed wherein a sequence of bytes representing a sinusoidal variation of a storage voltage is memorized. The memory store is addressed sequentially by the output of a counter and the memory content is applied to a fast digital-to-analog converter (DAC). When the clock is interrupted, the DAC output is held at a constant value corresponding to the appropriate memory content. This first method allowed to confine ions with a radio-frequency signal of 160 kHz generated digitally and to detect them at the end of the storage.

The subject of this article is the chopping of the trapping potential using an original electronic device. This acts to chop the rf voltage (V_{ac} cos Ωt) at a zero-crossing point at the instant $t = t_0$ and during a sufficiently long time that all the ions freely escape from the trap. The quality of the interruption process has been monitored by the measurement and simulation of the time-of-flight profile of the confined ions.

The drawback of this method is that the signal is weaker than the one obtained after the application of an extraction pulse; but its advantage is that the instantaneous kinetic energy is not disturbed by the ejection process. This method is also more sensitive in case of small ion kinetic energies.

This detection method permits the acquisition of a time-of-flight profile which can be associated to a 3D simulation of about 10^6 ion paths through the experimental setup in order to deduce the average kinetic energy of the ion cloud. In this simulation, we may take into account the possible overshoot (residual voltage named V_{res}), adding to the U_{dc} voltage (corresponding to the a_z parameter), to form the total voltage present on the ring after interrupting the radio frequency.

In this article, we first describe the apparatus used to obtain time-of-flight profiles and the experimental realization of ion ejection itself; second, we present in detail the improvements made in the existing model [6] in order to use it for the whole range of experimental cases (constant and positive/negative or zero V_{res} and time-dependent V_{res}).

2. Experimental

The work presented here has been carried out with N^+ ions confined in a Paul trap in the presence of molecular nitrogen at an ambient pressure of $\sim 10^{-8}$ mbar. Since the apparatus has been described in detail previously [7], only the essential points are presented here.

A Paul trap, an electron gun and an ion detection system are contained in an UHV vessel of volume 2.5 L. The pressure is monitored with a mass filter (Balzers QMG064) and a Bayard–Alpert gauge. We expect that electron impact ionization of N_2 creates N_2^+ (80%), N^+ (20%), and N_2^{2+} (<1%) inside the trap.

The ion trap is formed from three hyperbolic electrodes fabricated from stainless steel. The ring electrode of radius $r_0 = 14$ mm has a total height of 30 mm. While the central 10 mm of the ring electrode had been machined out and the electrode surface replaced by tantalum mesh (this aperture has no use in the experiments described here). The two end-cap electrodes that were separated by a distance $2z_0$ equal to 20 mm, were 35 mm in width and were grounded. The central region of diameter 25 mm of each end-cap electrode was replaced by a mesh to permit the passage of electrons and ions during the ionization and ion detection, respectively. A potential $V(t) =$

$U_{dc} + V_{ac} \cos \Omega t$ was applied to the ring electrode throughout the ion storage period.

The working point a_z, q_z of a given ion species depends upon the values of U_{dc}, V_{ac}, and Ω. For the experiments described here, the value of a_z was varied so that only N^+ and N_2^{2+}, having identical mass/charge ratios, remained confined in the ion trap. Typically, operating parameters could be varied to cover a large range of q_z values, $0.36 < q_z < 0.6$.

The entry grid of the electron multiplier (EM) (ET AF151 1G) was held at a high negative value, V_{HT}, in the range from -2000 to -1000 V, and was located on the z axis of the ion trap some 38 mm above the center of the ion trap. This first dynode has a rectangular opening of 12 mm $\times$ 7 mm. A supplementary grid of diameter 12 mm was mounted 8 mm in front of the EM and was grounded. In this way, ions passing through the end-cap electrode traverse a field-free region protected from the high voltage on the EM. Beyond the supplementary grid, ions are accelerated strongly towards the EM (Fig. 1).

Two rf generators were constructed so as to produce rf drive potentials, one oscillating at $\Omega/2\pi$ equal to 1.0 MHz and the other at 1.5 MHz. These generators are based on the principle illustrated in Fig. 2. Here, the alternating voltage is delivered by a step-up transformer (T) syntonized at the confinement frequency, $\Omega/2\pi$, and excited by a class A amplifier. The alternating voltage is applied to the ring electrode whereas the end-cap electrodes are grounded, in the most symmetrical manner possible, through the secondary of another transformer eventually used for the application of an alternating or "tickle" voltage [8].

The cutoff electronics consist of a bridge of fast, high inverse voltage (V_R) diodes. The transformer output is applied to one diagonal of this bridge and the other diagonal delivers the rectified value of the confinement voltage that polarizes a metal–oxide–semiconductor field-effect transistor (MOSFET) (M) selected for its high drain-to-source voltage (V_{DS}) and its low static on-state resistance ($r_{DS(on)}$) from the drain to the source. The field-effect transistor M is controlled through an optocoupler. During saturation of this transistor, the small conduction resistance $r_{DS(on)}$ short circuits the transformer output (with a high internal resistance). The phase of the control signal is adjusted very precisely, relative to the phase of the trapping voltage, so as to obtain the optimal cutoff. Optimization of this phase shift offers the best compromise between a precise cutoff at $\Omega t_0 = \pi/2 + 2k\pi$ and minimal overshoot of the rf voltage. Due to the rf phase chosen for the cutoff this overshoot or residual voltage (V_{res}), still present after the chopping, is always negative. Even if it is impossible to complete the short circuit or to chop instantaneously (principally due to the nonzero MOSFET resistance $r_{DS(on)}$ and residual inductive effects in the chopping circuit), V_{res} remains quadrupolar and it can be easily modeled and included in the simulation program.

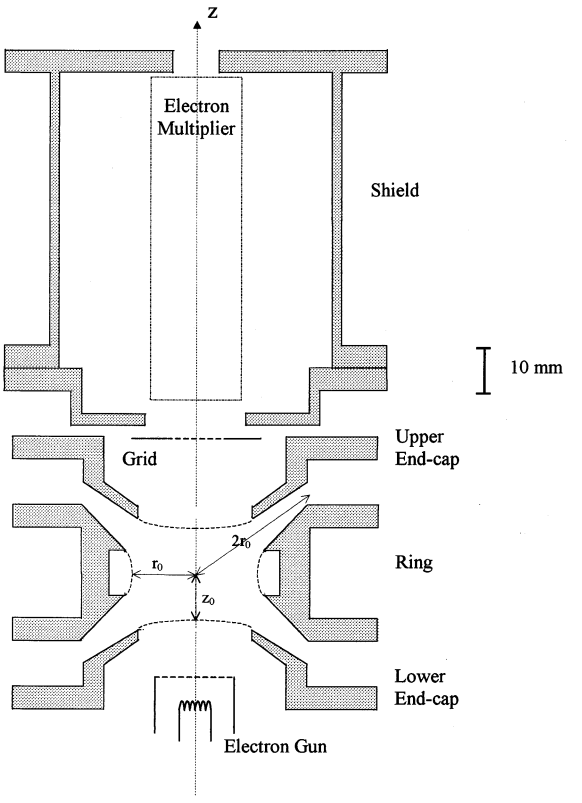

Fig. 1. Schematic cross-section of the experimental set-up.

Typically, an experimental sequence consist in creating ions by electron impact during 150 ms and letting them evolve in the trapping potential during 400 ms until the storage voltage is turned off.

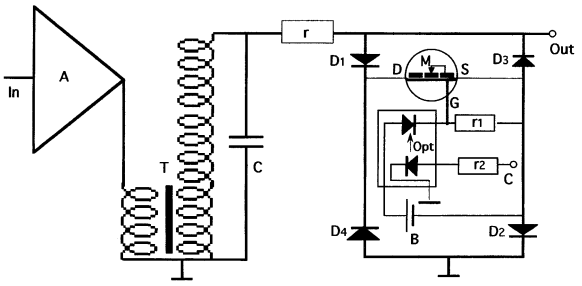

Fig. 2. Basic electronic circuit for the generation and interruption of the storage voltage. The analogic signal is applied to the input IN of the A amplifier; this one excites a transformer T (with internal resistor r and syntonized at the radio frequency). One of the diagonals of the bridge of fast diodes ($D_1 \cdots D_4$) can be short circuited by the conduction of the MOSFET (M) being under the control of the PC. OUT is applied to the ring electrode of the trap and delivers the radio-frequency. A: amplifier, T: step-up voltage transformer, C: variable capacitor, D_1, D_2, D_3, D_4: diodes, Opt: optocoupler (6N137), M: MOSFET (high-voltage MOSFET, i.e. 25K1120: $V_{DS} = 1000$ V, $r_{DS} = 1.8\ \Omega$).

The interruption of the rf voltage is maintained for some 10 μs so as to allow ions to escape from the ion trap. Ions having favorable positions and velocities will leave the ion trap through the upper end-cap electrode and may reach the first dynode of the EM. The current delivered by the EM is amplified by a charge amplifier. The signal obtained, proportional to the trapped ion number, can be visualized directly on a digital oscilloscope (Tektronix 2221A) that is synchronized to the rf voltage interruption time, t_0, and communicates with a PC (through an IEEE 488 interface). This PC is also used to monitor the entire timing sequence of each experiment via an analog/digital interface (AD RTI815). A time-of-flight profile is obtained in the form of a histogram of ion number reaching the detector in each successive time interval. This experimental profile can be characterized by different parameters: the arrival time of the first ion (t_{min}), the full-width at half-maximum of the profile (FWHM) (Δt, $\Delta t = t_2$-t_1) and the time corresponding to the maximum of the profile (t_{max}). We observed very good reproducibility of the measurements in all of the explored experimental conditions. This can be expressed by a low relative uncertainty for the different characteristic times: less than 2% for t_1 and t_2; of the order of 3%–4% for t_{min} and between 5% and 10% for t_{max} (these statistics were obtained from 20 profiles and for different working points). Each profile is peculiar to the kinetic energy distribution of the ions in the ion cloud when the storage field was interrupted. A simulation program, whereby ion trajectories through the experimental apparatus are calculated, permits reproduction of the experimental profile from which an average kinetic energy can be determined.

3. Time-of-flight method

The complete simulation is based on the hypothesis that ion spatial and ion velocity distributions are Gaussian. This hypothesis has been confirmed by numerous observations [9,10] and theoretical work [11]. Ion–ion collisions and ion–neutral collisions lead to the rapid thermalization of the ion cloud produced by electron impact: the cloud is characterized by an average kinetic energy since the energy itself oscillates at the storage frequency. However, the effects of space charge and ion–neutral collisions are sufficiently weak so that their omission from the simulation is justified. In order to obtain the best possible agreement between experimental and simulated profiles, it was necessary to monitor the ion number (about 10^5) in order to reduce the space-charge effects and to work at a relatively low pressure of neutrals [typically, $p(N_2) < 2 \times 10^{-8}$ mbar) so as to minimize the effects of ion-loss processes.

Couplings between radial and axial motions and between micro- and macromotions arise due to space charge and anharmonicities in the rf trapping field produced by imperfections in the ideal geometry of the ion trap. Such couplings can drastically modify the dynamics of stored ions. However, in the simulation, it was assumed that the rf trapping field is purely quadrupolar. In order for this principal hypothesis to be fulfilled in practice, it was necessary to work far from the resonance conditions predicted by theory [12] and observed in several experimental apparatuses (for instance, Refs. [7,13,14]) and with an ion cloud such that the majority of ions are stored near the center of the trap where they experience, only weakly,

the effects of nonlinearities. Hence working points were chosen that correspond to stable ion trajectories and under conditions where expansion of the ion cloud was minimized. If, on occasion, those precautions are not taken, the experimental profiles are greatly reduced in signal intensity and their falling edge is curtailed sharply. Such observations occur because the effects of nonlinear resonances. Attempts to match these profiles by simulation were not successful. Therefore, it cannot be assumed that the trapped ions detected in these experiments may be characterized by Gaussian distributions with respect to space and velocity. Then, observations of large differences between numerical and experimental profiles can be the sign of the nonrespect of the simulation hypothesis and can be used as a controller of nonlinear conditions.

For the case of ion storage in an ideal Paul trap, the standard deviations of the instantaneous position and velocity distributions $\sigma_u(t)$ and $\sigma_{\dot{u}}(t)$, respectively, can be calculated numerically at any instant (in particular, at zero rf phase, where the distributions are decorrelated) and for any direction, $u = x, y, z$, from the confinement conditions and the rf-averaged value (E_{lab}) of the ion kinetic energy, $\boldsymbol{E}_{\text{lab}}$

$$\sigma_{\dot{u}}(t) = \sigma_{0u}\sqrt{C_u^2(t) + D_u^2(t)} \tag{1}$$

$$\sigma_u(t) = \frac{\sigma_{0u}}{\omega_u}\sqrt{A_u^2(t) + B_u^2(t)} \tag{2}$$

where $\sigma_{0x} = \sigma_{0y}$ and $\sigma_{0z} = c_A\,\sigma_{0x}$ (C_A is a coefficient representing the anisotropy of the ion cloud) A_u, B_u, C_u, D_u are periodic functions of t

$$E_{\text{lab}} = \langle \mathbf{E}_{\text{lab}}(t)\rangle_{2\pi/\Omega} = \frac{m}{2}\left(2\langle\sigma_{\dot{x}}^2(t)\rangle + \langle\sigma_{\dot{z}}^2(t)\rangle\right) \tag{3}$$

An initial population of n N^+ ions, characterized by Gaussian spatial and velocity distributions with given dispersions $\sigma_u(0)$ and $\sigma_{\dot{u}}(0)$, respectively, is generated using the Box–Müller technique [15]. Positions and velocities of n ions are generated at $t = 0$ and the trajectory of each particle is calculated.

Until the interruption of the rf voltage at $t = t_0$, ion motion is assumed to be simply governed by three uncoupled Mathieu equations for which analytical solutions are well known [16]. For an instant $t < t_0$, the following relations can be deduced from those equations and applied to calculate positions and velocities at any instant:

$$\begin{aligned} u_i(t) = {} & \frac{u_i(0)}{A_u(0)}\left[A_u(t)\cos\omega_u t - B_u(t)\sin\omega_u t\right] \\ & + \frac{\dot{u}_t(0)}{\omega_u D_u(0)}\left[B_u(t)\cos\omega_u t\right. \\ & \left. + A_u(t)\sin\omega_u t\right] \end{aligned} \tag{4}$$

$$\begin{aligned} \dot{u}_i(t) = {} & -\frac{u_i(0)\omega_u}{A_u(0)}\left[C_u(t)\cos\omega_u t\right. \\ & \left. + D_u(t)\sin\omega_u t\right] + \frac{\dot{u}_i(0)}{D_u(0)} \\ & \times\left[D_u(t)\cos\omega_u t - C_u(t)\sin\omega_u t\right] \end{aligned} \tag{5}$$

When the rf voltage has been turned off and for $\Omega/2\pi = 1$ MHz, the residual voltage V_{res} remaining on the ring electrode can be approximated to a constant. For this case, the differential equations describing ion motion between $t = t_0$ and the time of arrival at the upper end-cap electrode are solved analytically for those ions having a velocity vector directed towards the EM input window. When $\Omega/2\pi = 1.5$ MHz and V_{ac} is correspondingly greater, V_{res} becomes of more importance and its time-dependent variation can no longer be neglected. V_{res} can be fitted to a very good approximation to a nth order polynomial ($n \geq 3$) as shown in Fig. 3. In this case, the equations of motion are solved with a fourth-order Runge–Kutta algorithm having as a variable step a fraction of the secular period of ion motion ($2\pi/\omega_u$).

Particles have a uniform and rectilinear motion between the upper end-cap electrode and the protective grid; beyond that point and for the remaining 8 mm, as mentioned previously, they are accelerated greatly towards the EM. When ions with a kinetic energy of 1 eV are considered, the time to cover this distance is not negligible compared to their total time-of-flight through the apparatus and so it is taken into account.

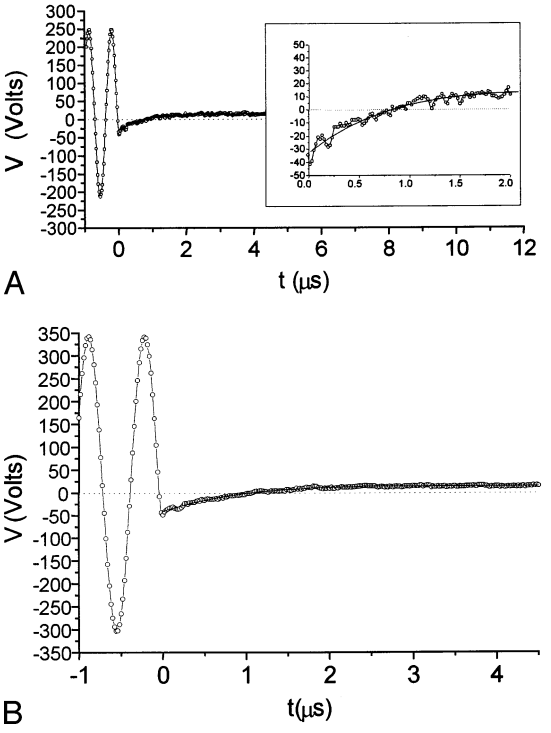

Fig. 3. (A) Cutoff signal and fit with sixth order polynomial for V_{ac} = 163.5 V_{rms}, U_{dc} = 18 V, and $\Omega/2\pi$ = 1.5 MHz (q_z = 0.358; a_z = −0.056), (B) Cutoff signal and fit with third order polynomial for V_{ac} = 228 V_{rms}, U_{dc} = 20 V, and $\Omega/2\pi$ = 1.5 MHz (q_z = 0.500; a_z = −0.062).

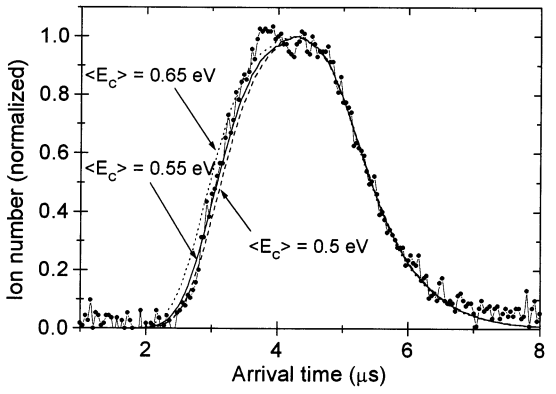

Fig. 4. Adjustment of an experimental profile (dots) obtained for V_{ac} = 110 V_{rms}, U_{dc} = 19 V, $\Omega/2\pi$ = 1 MHz (q_z = 0.543; a_z = −0.132) with three profiles calculated with E_{lab} = 0.5, 0.55, 0.65 eV and c_A = 1.

4. Results

The arrival time of a particle at the detector can be calculated as described above. Once allowance is made for the response time of the detector, a histogram can be constructed from the global sample of ions created initially. It is constituted by 500 channels corresponding to time intervals of 0.04 μs. The experimental profile is compared, in turn, with this histogram in order to justify the arbitrarily chosen initial conditions expressed by the parameters E_{lab} (laboratory frame) and c_A, where c_A varies little from unity [11]. In this comparison, attention was focused on the adjustment of the rising edge of the signal (risetime characterized by t_{min} and t_1), the maximum (t_{max}) and the FWHM (Δt) of the profile. The falling edge of the signal (when $t \gg t_2$) does not seem to be an important criterion because ions forming the trail of the experimental profile are really sensitive to parasitic voltages which are not taken into account in simulation. By varying E_{lab} and c_A, the risetime, the time corresponding to the maximum and the width of the simulation histogram are modified until the histogram is fitted to the experimental profile. Fig. 4 shows some results of this approach: three modified histograms are shown, corresponding to E_{lab} values of 0.5, 0.55, and 0.65 eV together with an experimental profile; it can be seen that the histogram for E_{lab} = 0.55 eV agrees well with the profile. (The decay of the histogram does not appear to be a sensitive function of E_{lab} for this working point.)

The simulation is able to follow small details of the experimental profile so that very good agreement can be obtained. In Fig. 5 is shown three examples of iteratively modified simulation histograms (solid line) superimposed on experimental profiles (dots); for those examples corresponding to different working points, best fits were obtained for a total mean energy equal to 0.5 eV with uncertainties of 0.1 eV at q_z = 0.358 (A), (2.0 ± 0.3) eV at q_z = 0.500 (B), and (2.45 ± 0.1) eV at q_z = 0.558 (C). Here, q_z values have been calculated from the experimental parameters V_{ac}, $\Omega/2\pi$ and r_0. We can note that the two first examples present the largest relative uncertainties; they correspond to cases where the residual voltage is quite high and time dependent. At last, the excess of

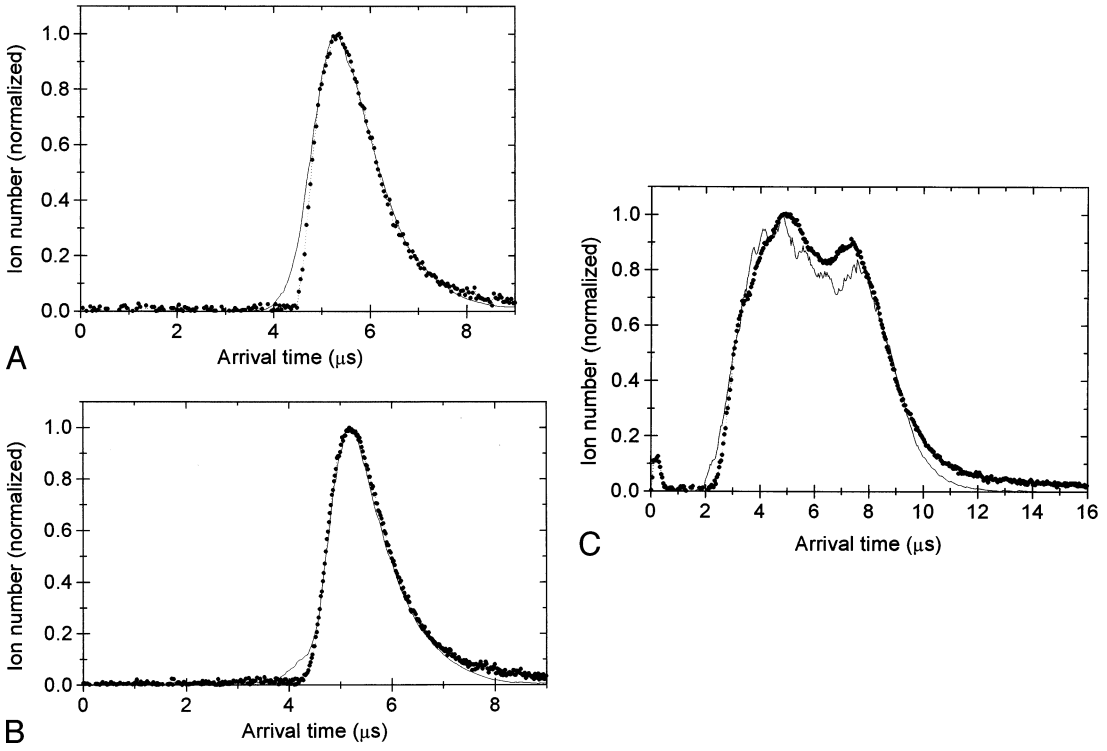

Fig. 5. Best adjustment (—) of experimental profiles (●) in case of time-dependent (A, B) or constant (C) residual voltage. (A) Experiment: V_{ac} = 163.5 V_{rms}, U_{dc} = 18 V, and $\Omega/2\pi$ = 1.5 MHz (q_z = 0.358; a_z = −0.056) simulation: E_{lab} = (0.5 ± 0.1) eV, c_A = 0.74; (B) experiment: V_{ac} = 228 V_{rms}, U_{dc} = 20 V, and $\Omega/2\pi$ = 1.5 MHz (q_z = 0.500; a_z = 0.062) simulation: E_{lab} = (2.0 ± 0.3) eV, c_A = 0.9; (C) experiment: V_{ac} = 113 V_{rms}, U_{dc} = 3 V, $\Omega/2\pi$ = 1 MHz, and V_{res} = 4 V (q_z = 0.558; a_z = −0.021) simulation: E_{lab} = (2.45 ± 0.1) eV, c_A = 1.

relatively high velocity ions that are shown in the simulation histogram can be explained by the fact that collisions occurring during the trapping time are not taken into account in the simulation. Such collisions can lead to a rapid loss of hot ions; clearly, such ions are not present in the experimental profiles.

5. Conclusion

An ion extraction technique in which the trapping potential is interrupted sharply has been described here. This technique has been applied under ion trapping conditions of high frequency with $\Omega/2\pi$ equal to 1.0 and 1.5 MHz and modestly high voltage of V_{ac} up to 700 V_{pp}. As a consequence of the interruption of the confining potential, ions can freely escape from the trap, a time-of-flight profile is collected by an EM. The kinetic energy of the ions has been determined using a simulation program, the agreement between simulation and experiment is a test for the quality of the chopping process. While the observed ion signal intensity with the interrupted trapping potential is less than that obtained when an extraction pulse is applied to an end-cap electrode, the method described here permits determination of the average kinetic energy of stored ions with resolution up to 0.1 eV.

If the frequency is greater than 1.5 MHz (corresponding to high voltages), the efficiency of the electronic cutoff system begins to deteriorate (V_{res} becomes difficult to minimize); actually, it appears that a limit of the method has been reached at this frequency. The energy imparted to the ions by the

residual voltage at the instant of the cutoff becomes dominant compared to the average ion cloud. This leads, of course, to larger uncertainties in the evaluation of the ion energy.

References

[1] R.E. March, J.F.J. Todd, Practical Aspects of Ion Trap Mass Spectrometry, CRC Series Modern Mass Spectrometry, CRC Press, Boca Raton, FL, 1995, Vols. 1–3.
[2] D.J. Wineland, J.C. Bergquist, D. Berkeland, J.J. Bollinger, F.C. Cruz, W.M. Itano, B.M. Jelenkoviæ, B.E. King, D.M. Meekhof, J.D. Miller, C. Monroe, M. Rauner, J.N. Tan, Application of Laser-Cooled Ions to Frequency Standards and Metrology, Proceedings of the 5th Symposium on Frequency Standards and Metrology, World Scientific, Singapore, 1996, pp. 11–19.
[3] P.H. Dawson, N.R. Whetten, J. Vac. Sci. Technol. 5 (1968) 11–18.
[4] M.D.N. Lunney, F. Buchinger, R.B. Moore, J. Mod. Opt. 39 (1992) 349–360.
[5] E.R. Mosburg, M. Vedel, Y. Zerega, F. Vedel, J. Andre, Int. J. Mass Spectrom. Ion Processes 77 (1987) 1–12.
[6] M. Vedel, M. Knoop, D. Lunney, I. Rebatel, F. Vedel, Phys. Rev. A 51 (1995) 2294–2300.
[7] M. Vedel, J. Rocher, M. Knoop, F. Vedel, Appl. Phys. B 66 (1998) 191–196.
[8] S.A. McLuckey, D.E. Goeringer, G.L. Glish, J. Am. Soc. Mass Spectrom. 2 (1991) 11–21.
[9] R. Iffländer, G. Werth, Metrologia 13 (1977) 167–170.
[10] R.D. Knight, M.D. Prior, Appl. Phys. 50 (1979) 3044–3049.
[11] F. Vedel, J. Andre, M. Vedel, G. Brincourt, Phys. Rev. A 27 (1983) 2321–2330.
[12] Y. Wang, J. Franzen, K.P. Wanczek, Int. J. Mass Spectrom. Ion Processes 124 (1993) 125–144.
J. Franzen, R.H. Gabling, M. Schubert, Y. Wang, Practical Aspects of Ion Trap Mass Spectrometry, CRC Series Modern Mass Spectrometry, CRC Press, Boca Raton, FL, 1995, Vol. 1, Chap. 3, pp. 49–167.
[13] F. Guidugli, P. Traldi, Rapid Commun. Mass Spectrom. 5 (1991) 343–348.
[14] R. Alheit, S. Kleineidam, F. Vedel, M. Vedel, G. Werth, Int. J. Mass Spectrom. Ion Processes 154 (1996) 155–169.
[15] J. M. Hammersley, C.D. Handscomb, Les Méthodes de Monte-Carlo, Monographie Dunod, Paris, 1967.
[16] R. Campbell, Théorie Génerale de l'Équation de Mathieu, Masson, Paris, 1955.